Available online at www.sciencedirect.com
ScienceDirect
Cement and Concrete Research 38 (2008) 449–458
Cement and Concrete Research

3D multi-scale modelling of mechanical behaviour of sound and leached mortar

F. Bernard, S. Kamali-Bernard *, W. Prince

Laboratoire de Génie Civil et Génie Mécanique (LGCGM), Institut National des Sciences Appliquées, 20 Avenue des Buttes de Coësmes, 35043 Rennes Cedex, France

Received 16 July 2007; accepted 29 November 2007

Abstract

A 3D multi-scale modelling of mechanical properties of cement-based materials approach is presented. The proposed approach provides a quantitative means to estimate and predict the mechanical properties of cement-based materials taking into account the eventual changes in the micro-structure. Two numerical tools are combined. First, the NIST's 3D model (CEMHYD3D) is used to generate a realistic 3D Representative Volume Element of cement-based materials at different scales. Then, multi-scale simulations are performed by using the FE software Abaqus for the calculation of the mechanical behaviour. The approach is then successfully applied to a specific mortar in order to determine firstly its mechanical behaviour under tensile and compression loadings and secondly the evolution of its Young's modulus under the leaching phenomenon. This evolution is a key parameter since the leaching may be critical for the mechanical integrity of concrete structures such as radioactive waste storage systems in which cement-based materials may be largely used. The numerical results of the modelling are consistent with the experimental ones.

Keywords: Mortar; Micro-structure; Modelling; Mechanical properties; Leaching

1. Introduction and methodology

Concrete is a heterogeneous material composed of a mixture of sand, aggregates embedded in a hardened cement paste. Three elementary scales of heterogeneity can be considered. On the macro-scale, large aggregates with Interfacial Transition Zone (ITZ) embedded in a matrix of mortar can typically be observed. This mortar consists of small sand particles bonded by cement paste. At this scale, called hereafter meso-scale, air voids are generally observed too. The third scale corresponds to the micro-scale which is the scale of the hydrated cement paste. This paste is a heterogeneous and complex porous medium in which the main solid phases are Calcium Silicate Hydrates (C–S–H), portlandite (Calcium Hydroxides or CH) and hydrated aluminates and sulfoaluminates phases. The solid phases are in chemical equilibrium with an interstitial solution that partially or totally fills the porosity.

The differences in mechanical properties of the various constituents at the different scales further increase the heterogeneity of cement-based materials. The stiffness and the strength of the different components influence the global stiffness and fracture behaviour of the material. The micro-structure of cement-based materials is too complex and random to allow for the development of exact analytical formulas that describe how the properties are related to the micro-structure. Besides, the only real alternative to empirical formulas is to use numerical methods.

The tremendous increase of computational capabilities has largely favoured the development of numerical simulation based on a more realistic explicit description of the material and specially its micro-structure [1]. Using such computational

* Corresponding author.
E-mail address: Siham.Kamali-Bernard@insa-rennes.fr (S. Kamali-Bernard).

0008-8846/$ - see front matter © 2008 Elsevier Ltd. All rights reserved.
doi:10.1016/j.cemconres.2007.11.015

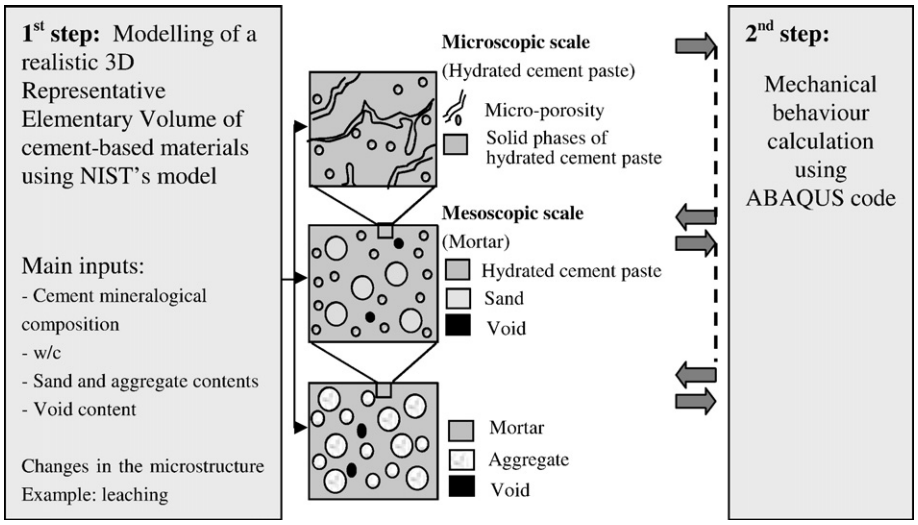

Fig. 1. Illustration scheme of the proposed 3D multi-scale numerical modelling approach for the determination of the mechanical behaviour of cement-based materials under mechanical and chemical loadings.

approaches has many advantages compared to more traditional methods, among them:

- the understanding of local deformation mechanisms, stress concentration and distribution in the constituents of composite materials;
- the finest prediction of the overall properties of heterogeneous materials. Numerical methods are more precise than homogenisation techniques in the case of complex global loading conditions (multiaxial, cyclic behaviour…) and when the properties of the constituents are highly contrasted (like in cement-based materials);
- the simulation of local damage processes: the computation of explicit micro-structures provides damage initiation which is not driven by mean values of stress and strain in each component. These local data can also be coupled to damage criteria or damage evolution equations to predict initiation and propagation of damage or cracks;
- the possibility to take into account the micro-structure evolution due to chemical reactions for example in order to study durability problems of concrete.

The outcomes of such computational approaches could then be used to derive material properties for modelling concrete as a homogeneous material to analyze structures.

For a few years, some attempts of heterogeneous modelling of cement-based materials have appeared. These works are most of time performed at meso-scale. Even if some of them present generated random aggregate structures closed to reality, they do not have real micro-structural considerations [2–4]. That is why they need experimental data to identify the constitutive laws of the different phases at this scale. A real multi-scale approach starting from micro-structure has been led at Delft University [5,6]. Lattice type models, have been introduced here to model concrete behaviour. This model is one of the most popular to explain fracture in cement based-materials, mainly because the simulated cracks are very realistic and resemble to a great detail the cracks observed in laboratory tests and in practice [7]. However this multi-scale modelling is performed in 2D and still has computational limitations, the stress–strain curves obtained on uniaxial tests (especially compression) remain until now not realistic [8].

In this paper, the proposed modelling consists in combining two 3D modern numerical tools. The aim is to show that starting from simulated micro-structure and with relatively simple mechanical considerations it is possible to reproduce correctly the mortar behaviour.

First, the NIST's 3D model (CEMHYD3D) is used to model a realistic 3D Representative Volume Element of cement-based materials at 2 different scales (cement paste, mortar). The voxelized images are then converted to Finite Elements Meshes compatible with the FE software Abaqus. This last one is then used to study the mechanical behaviour of the considered 3D Representative Elementary Volume. The outcome of a lower scale is then used as input at a higher scale. This approach is illustrated in Fig. 1.

Table 1
Composition of the studied mortar

Composition in kg/m^3	
Cement CEM I 42.5	639
Sand S1 (0.8–3.15)	414
Sand S2 (0.16–0.2)	966
Water	256

Table 2
Mineralogical composition of the portland cement used in this study given in % of weight content [3]

C_3S	C_2S	C_3A	C_4AF	Gypsum
53%	19.4%	7.2%	7.9%	5.5%

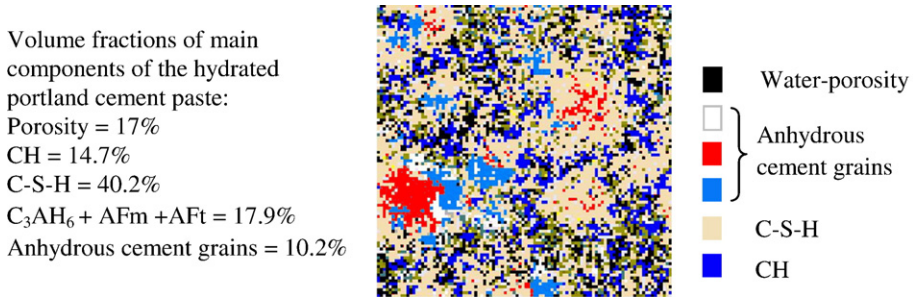

Fig. 2. 2D cross section of the micro-structure of the hardened cement paste obtained using CEMHYD3D model (resolution: 1 μm/pixel).

In this paper, the proposed approach is applied:

- Firstly, to determine the mechanical behaviour of a specific mature mortar with water-to-cement ratio 0.4 that has previously been investigated experimentally. The micro-scale of the cement paste and the meso-scale of the mortar are considered. Tensile and compression loadings are investigated.
- Secondly, to evaluate the effect of the leaching phenomenon on the evolution of the Young's modulus of the considered mortar. The numerical results are then compared to the experimental ones.

2. Application no. 1: modelling of the mechanical behaviour of a specific mortar

2.1. Mortar composition

The mortar modelled in this paper has already been investigated experimentally in Kamali's and Le Bellego's works [9,10]. Its composition is given in Table 1. It contains two different sands S1 and S2 and has a water to cement ratio w/c equal to 0.4. A portland cement, CEM I 42.5 type, is used and its mineralogical composition is given in Table 2. The following study is performed for well-hydrated material.

2.2. Step 1: construction of the micro-structure of the cement paste and meso-structure of the mortar

At the micro-scale, the hydrated cement paste corresponding to the considered mortar is modelled using NIST's CEMHYD3D code. This well-known model has been described in detail previously [11]. It is composed of two main programs. The first one allows creating initial non-hydrated 3D cement voxelized image taking into account the particle size distribution and the mineralogical composition of the considered portland cement as well as the water-to-cement (w/c) ratio. A resolution of 1 μm/voxel is used in this paper and a cube of $100\times100\times100$ voxels of water and cement mixture is generated. The second program based on cellular-automata techniques hydrates the initial 3D micro-structure and generates a 3D hydrated cement paste. The both programs are of random nature. Fig. 2 shows a 2D cross section of the modelled micro-structure.

At the meso-scale and using again the first program as for the micro-scale, the mortar is modelled as a continuum of cement paste containing spherical aggregates approaching a size distribution corresponding to the sand of the real mortar. A 5 mm side elementary cube of mortar containing a quantity Q_1 of spheres of diameter D_1, a quantity Q_2 of spheres of diameter D_2 and a quantity Q_3 of spheres of diameter D_3 is generated. The first spheres represent the grains of sand S_1, the second, the grains of sand S_2 and the third the air voids. The quantities Q_1 and Q_2 are calculated from the mass contents of sands S_1 and S_2 (414 kg/m^3 and 966 kg/m^3 of mortar). D_1, D_2 and D_3 are respectively the considered values of the diameters of sands S_1 and S_2 and air voids. They are respectively equal to 1.125 mm, 0.125 mm and 0.375 mm (particle size distributions of sands are not completely known). The air volume content of the mortar is taken equal to 3% [12]. The remaining volume corresponds to the cement paste. ITZ with one voxel depth is considered around the largest grains which correspond to sand S1. Fig. 3 shows a

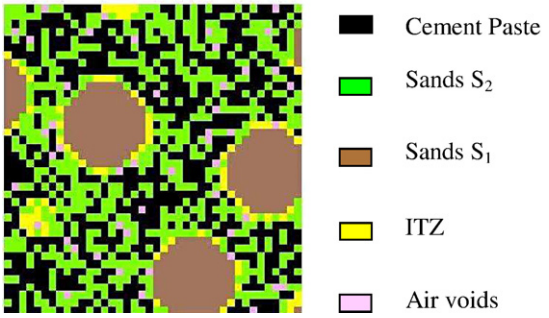

Fig. 3. 2D image of the meso-structure of mortar showing the different components considered in this study (resolution: 125 μm/voxel).

Table 3
Young's modulus, *E*, and Poisson's ratio, *v*, values of the principal phases used in modelling [16]

Phases	*E* (GPa)	*v*	References
C_3S	117.6	0.314	[17]
C_2S	117.6	0.314	
C_3A	117.6	0.314	
C_4AF	117.6	0.314	
Gypsum	45.7	0.33	[18,19]
Portlandite	42.3	0.324	[20]
C–S–H	22.4	0.25	[21]
C–S–H_{pozz}	22.4	0.25	
Afm	42.3	0.324	
Aft	22.4	0.25	
Empty porosity	0	0	

2D cross section of the generated meso-structure. A resolution of 125 μm/voxel is used.

Due to computational reasons and to the used regular mesh, this side is several times higher than typical ITZ thickness equal to about 20 μm. Homogenised values are calculated and affected to this zone.

2.3. Step 2: mechanical modelling of mortar under tensile and compression loadings

At this step, because of the limitation by the memory capacity accorded to the software pre-processor, elementary cubes of 50 voxels side for cement paste and 40 voxels side for mortar are extracted from CEMHYD3D images. Then these extracted voxelized images are used by the FE software Abaqus. Each cubic voxel in the 3D micro-structure and meso-structure is mapped into a solid linear finite element. The mesh is regular and air voids are explicitly represented but are not meshed. Elementary cubes of 50 μm side for cement paste and 5 mm side for mortar are then considered. At the micro-scale, a finite element has a volume equal to 1 μm^3 (cube of 1 μm side) and 125^3 μm^3 at meso-scale (cube of 125 μm side). According to Kanit et al. [13], the representativeness of these volume elements is checked imposing different boundary conditions: kinematics (a displacement is imposed at the boundary) or stress (a traction vector is prescribed at the boundary) uniform conditions.

These last conclusions are in good agreement with results of Smilauer [14] who has concluded that 50 μm is a reasonable representative size for a typical cement paste. At the mortar level, a representative size of 5 mm is in the range of values generally used (1–10 mm) [14].

The outcomes of the FE simulation at the micro-scale (cement paste) is used as input data at the meso-scale (mortar) modelling. For all the following simulations, the software Abaqus with classical integration rules is used [15].

2.3.1. Micro-scale: cement paste

At this scale, the modelling aims to obtain the response of the Representative Volume Element (RVE) to a tensile loading. This outcome is obtained by imposing a displacement on two opposite faces of the REV mesh. The global load (sum of the reaction forces at the different nodes) and the total displacement

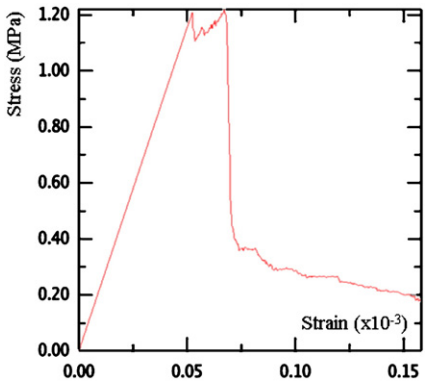

Fig. 4. Stress–strain curve obtained for the considered cement paste under tension loading.

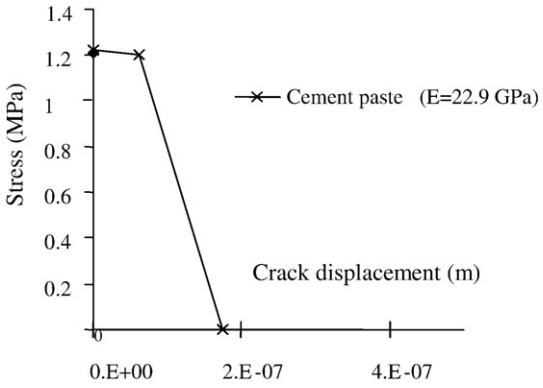

Fig. 5. Post failure stress-displacement curves of the studied hardened cement paste under tensile loading.

are then compiled and divided by the section surface and the initial length respectively. Then, one is able to draw the homogenized stress–strain curve. The Poisson coefficient is determined by homogenization of the displacement on the other faces.

The properties of each phase contained in the cement paste are considered in such a way that hydrates and non-hydrated cement phases are assumed to be perfectly elastic. The values of the elastic modulus and of the Poisson coefficient of these different phases are taken from the literature. They are obtained from nano-indentation measurements and are presented in Table 3. Corresponding references of the literature are indicated too [16–21].

The tensile strength f_t is taken proportional to the stiffness values ($f_t = E/10{,}000$) as in Schlangen [6]. A Rankine criterion is used to model the failure of the different phases. It states that the failure takes place when the maximal principal stress exceeds the tensile strength of the phase.

The simulation is carried out for the considered cement paste and results are plotted as shown in Fig. 4. On a single 32-bit PC (Processor: 2.8 GHz, RAM memory: 2.62 GB), the simulation times reaches about 1.5 day.

2.3.2. Meso-scale: mortar

At the meso-scale, failure is supposed to be the consequence of crack initiation and propagation at highly localized regions under large tensile stresses concentration. Thus only the tensile

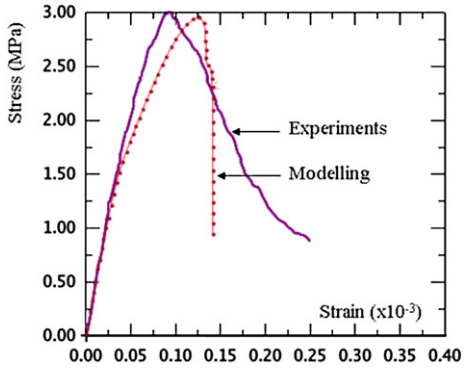

Fig. 6. Stress–strain curves in tension for the studied mortar — comparison modelling and experiments.

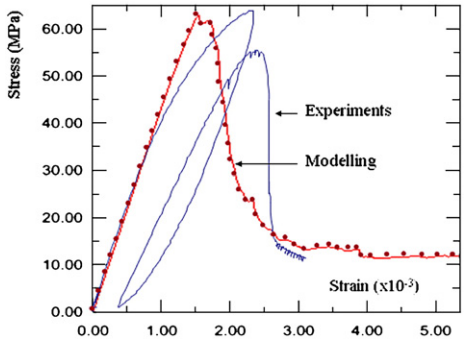

Fig. 7. Numerical stress–strain curves in compression for the studied mortar and comparison with experiments.

behaviour of the hardened cement paste is needed. Failure in compression is then assumed to be the consequence of tensile eigenstresses resulting from restrained deformations due to the heterogeneous meso-structure of mortar.

In all simulations, a cohesive crack model is used to represent the tensile behaviour of hardened cement paste [22]. Abaqus assumed that cracks are fixed and orthogonal to the direction of the maximum principal stress. A Rankine criterion is used to detect crack initiation. The specification of the post failure tensile behaviour needs to enter the post failure stress as a tabular function of displacement across the crack (instead of strain which can introduce mesh sensitivity) [15]. This post failure stress-displacement curve is obtained by inverse identification. The identification is performed comparing results of simulation of tensile tests on a 5 mm side cube of homogeneous hardened cement paste (simulations in which we impose various post failure behaviours) and results of previous simulations on heterogeneous media. This side is chosen to be compatible with the displacement needed in the model.

Elastic properties (Young's modulus and Poisson coefficient), tensile strength and post failure tensile stress-displacement are the unique data that are transferred from cement paste to mortar.

Besides, a characteristic length is introduced in the software Abaqus to regularize the smeared continuum models and attenuate the sensitivity of the results to mesh density [15]. This characteristic length is based on the element geometry: for solid elements it is equal to the cube root of the integration point volume. The characteristic length allows to pass from the strain to the relative displacement.

The behaviour of the cement paste is plotted in Fig. 5. Remaining tensile strength at the end of the test is neglected.

The compressive behaviour of the hardened cement paste is assumed to be always linear elastic. As prescribed in Abaqus [15], in absence of test data, the post cracking shear behaviour is assumed to go linearly to zero at the same crack opening displacement used for tension model. The sand particles are assumed to follow the same type of behaviour. Their Young's modulus is equal to 80 GPa and the Poisson coefficient value is 0.2. Their post failure stress-displacement curve is obtained from their fracture energy value (120 N/m) [23].

Because of a lack of data on the tensile strength and the inelastic behaviour of the ITZ, the presence of this zone is not taken into account at this stage of the paper. Further research is needed to evaluate precisely its behaviour.

In order to avoid any problems of convergence due to excessive distortion of elements which can no longer carry stress, a brittle failure criterion called "element kill" [15] technique is used. Then when the local cracking displacement reaches a critical value, all the stress components are set to zero and the corresponding element is removed from the mesh. On a single 32-bit PC (Processor: 2.8 GHz, RAM memory: 2.62 GB) with a memory consumption of 1.5 GB (respectively 4.3 GB) the simulation time for a tensile test (respectively compressive test) reaches 1.5 day (respectively 4 days).

2.4. Modelling results and comparison with experiments

The stress–strain curves corresponding to tensile and compression loadings are obtained by imposing respectively a positive and a negative displacement on a Representative Volume Element of mortar with free boundary conditions. Kamali and Le Bellego's tensile and compression experiments were carried on 140 mm height and 70 mm diameter samples of mortar [9,10]. Figs. 6 and 7 present comparisons between modelling and experimental results.

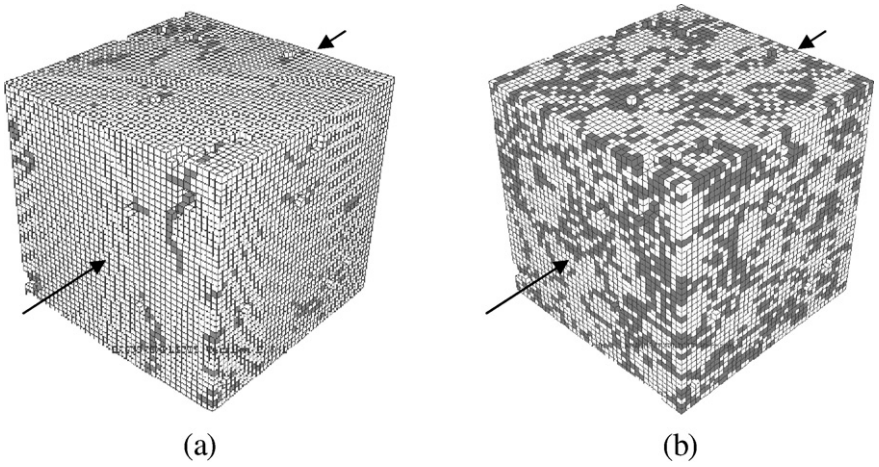

Fig. 8. Crack patterns (dark voxels) of the considered mortar obtained by computational calculations under compression (a) just before the peak and (b) after the peak.

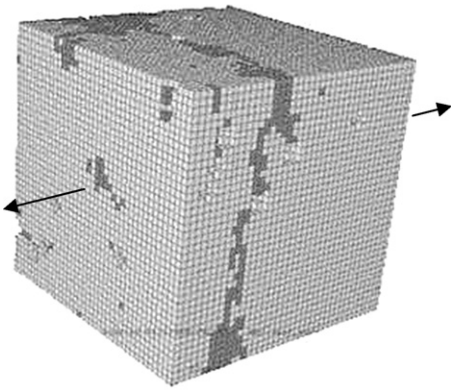

Fig. 9. Crack patterns (dark voxels) of the considered mortar obtained by computational calculations under tension loading.

The comparisons show realistic stress–strain responses. Elastic parameters and strength are correctly represented. For both simulations, non-linearities are well described even if the tensile behaviour seems to be a little bit too brittle and if compressive damage evolution before the peak differs slightly from the experiments. The brittle behaviour in tension can be explained by the brittle failure criterion which is however interesting for the convergence of the computations. In compression, a possible reason for the differences between experimental and modelled results is the absence of the Interfacial Transition Zone in modelling. Indeed when the mortar is subjected to the compressive loading, concentration of shear and tensile stresses occurs at interfaces due to differences in elastic modulus of the mortar components. ITZ micro-cracking increases [24,25] leading certainly to a fall of the elastic modulus. However, as mentioned by Akçaoglu et al. [25], the interfacial bond has little influence on compressive strength [25], that is probably why no real difference has been found on this parameter between experiments and our modelling in this present study.

Despite of these slight differences, crack patterns are very realistic before and after the peak. Indeed, failure is normal to the solicitation axis in tension and is more diffuse in compression as shown in Figs. 8 and 9.

3. Application no. 2: effect of the leaching on the evolution of the elastic modulus of mortar

It has been shown by several authors that leaching involves a decrease of many physical properties of cement-based materials: elastic modulus, compressive strength [9,10,26], internal friction angle [27]. Recently, Kamali et al. [16] have shown that the leaching of the portlandite phase can involve a reduction by about 48% of the elastic modulus of a portland cement paste with water-to-cement ratio equal to 0.4. This result is in a good agreement with Carde's experimental data [26].

In this paper the meso-scale of mortar is investigated and the effect of leaching phenomenon on the evolution of the Young's modulus is modelled. Kamali's and Le Bellego's experiments are again used and simulated [9,10]. In these experiments, cylindrical samples of 140 mm height and 70 mm diameter made of the same mortar as studied in paragraph 2 have been leached. An accelerated leaching test within ammonium nitrate solution (NH_4NO_3) has been used. Several samples have been submitted to 1D radial leaching during different time periods: 0, 28, 56 and 98 days. Fig. 10 illustrates the evolution of the degraded zone with the duration of immersion in ammonium nitrate solution. The leached samples are then tested under compression and tensile loadings [9,10].

3.1. Step 1: modelling of the leached material

It is well-known that the altered zone of cement-based material submitted to one-dimensional leaching (pure water or ammonium nitrate solution) is composed of different zones with constant mineralogy delimited by dissolution-precipitation fronts [12,26,28,29]. In order to be able to calculate the characteristics of the various zones, it is initially necessary to identify how many zones should be considered and what are their compositions.

3.1.1. Identification of the various zones of the leached mortar and their composition

Several studies have shown that portlandite is the first mineral to be dissolved followed by hydrated aluminates and sulfoaluminates phases and gradual decalcification of C–S–H [12,26,28,29]. The surface zone is much altered; it is made of

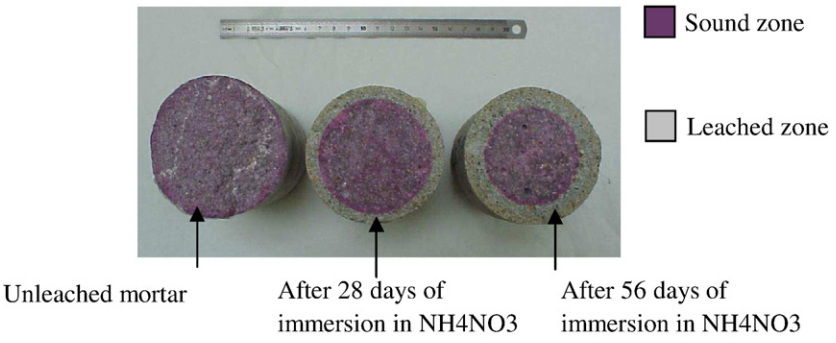

Fig. 10. Horizontal cross sections of the leached samples of mortar.

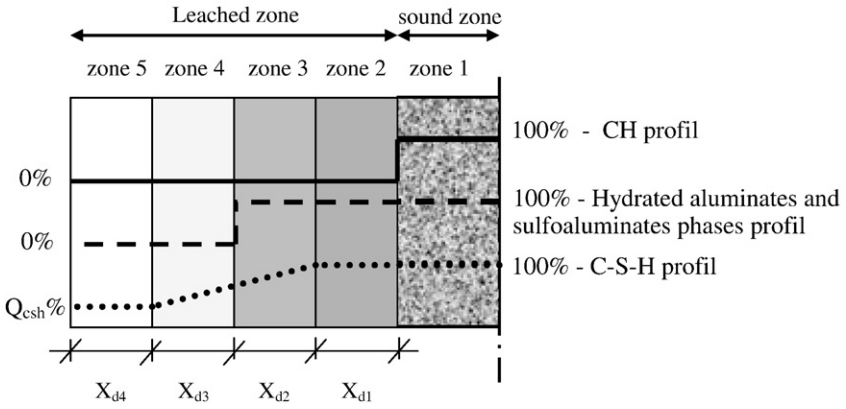

Fig. 11. The various considered zones and their composition.

highly decalcified C–S–H. From these reports, a model describing the composition of the cement paste degraded with ammonium nitrate solution can be proposed. Five zones are defined and are illustrated in Fig. 11:

- Zone 1: sound zone
- Zone 2: zone where portlandite (CH) is totally dissolved
- Zone 3: zone where portlandite is totally dissolved and C–S–H begin to be decalcified (the C–S–H decalcification is taken into account by a partial and linear dissolution)
- Zone 4: zone where portlandite, hydrated aluminates and sulfoaluminates phases are totally dissolved and C–S–H continue to be decalcified (linear dissolution of C–S–H)
- Zone 5: much altered zone, only made of a highly decalcified C–S–H.

The rate of C–S–H in the surface zone, Q_{csh}, is estimated from the calcium contents in this zone measured by an electronic micro-probe and given by Le Bellego [10]. According to this experimental study, this rate increases with the leaching duration. In this paper, value of 60%, 75% and 90% after respectively 28, 56 and 98 days are taken into account. In addition, according to Adenot [28], the various dissolution/precipitation fronts (X_{d1}, X_{d2}, X_{d3}, X_{d4}) are proportional to a square root of time as long as an unleached zone exists, the composition of the aggressive solution remains constant and the one-dimensional leaching is checked.

The identification of X_{d1}, X_{d2}, X_{d3}, X_{d4} values after any leaching duration is easily deduced from their values at a given time. Table 4 summaries the various fronts positions for the different leaching durations retained in this study and corresponding to Le Bellego's (28, 56 and 98 days) experiments as well as the composition of the various zones.

Table 4 allows the identification of 10 different leached micro-structures: one micro-structure without portlandite corresponding to zone 2, and three different leached micro-structures for each of the following zones (zone 3, zone 4 and zone 5). In order to deduce the homogenised properties of the leached samples, it is necessary to calculate physical characteristics, elastic modulus and Poisson coefficient of the 11 different micro-structures including the sound zone (zone 1).

3.1.2. Micro-structure modelling of leached zones of cement paste

The effect of the complete leaching of a component is taken into account by giving to this component the properties of the water. The partial and random dissolution of C–S–H is made before the modelling by Abaqus. Fig. 12 shows a 2D cross section of the micro-structure of a leached zone of the cement paste. It corresponds to Fig. 1 after leaching of CH,

Table 4
X_{di} values and composition of each zone

Leaching duration	X_{di} in mm				Leached components			
	X_{d1}	X_{d2}	X_{d3}	X_{d4}	Zone 2	Zone 3	Zone 4	Zone 5
28 days	8.9	8.0	5.9	3.7	100% CH	100% CH 15.2% C–S–H	100% CH 45.2% C–S–H 100% Alu[a]	100% CH 60% C–S–H 100% Alu[a]
56 days	12.6	11.3	8.3	5.3	100% CH	100% CH 20% C–S–H	100% CH 56.5% C–S–H 100% Alu[a]	100% CH 75% C–S–H 100% Alu[a]
98 days	16.7	15	11	7	100% CH	100% CH 25% C–S–H	100% CH 68.5% C–S–H 100% Alu[a]	100% CH 90% C–S–H 100% Alu[a]

[a] Hydrated aluminates and sulfoaluminates phases.

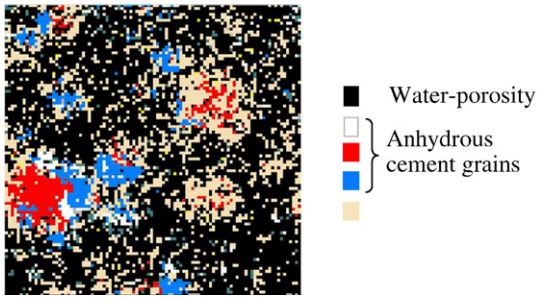

Fig. 12. 2D cross section of the micro-structure of a leached paste zone corresponding to cement paste with CH, Alu and 45.2% of C–S–H leached.

hydrated aluminates and sulfoaluminates phases and 45.2% of C–S–H.

3.2. Step 2: modelling of the Young's modulus of the leached mortar samples

3.2.1. Young's modulus of the leached cement paste zones

The Young's moduli of the leached cement paste zones are obtained with Abaqus as described previously. Simulations are performed on 50 µm side Representative Volume Element with a resolution of 1 µm/voxel and with free boundary conditions. Table 5 gives the calculated values and variations with respect to the initial value.

3.2.2. Young's modulus of the leached mortar zones

The calculation of the elastic modulus of the 11 mortar zones corresponding to the 11 cement paste zones previously simulated is carried out with Abaqus by assigning to the cement paste and to the sands particles the characteristics calculated previously (as used in [24]). In this part, simulations are performed on 5 mm side RVEs with free boundary conditions. Each edge is divided into 40 elements, leading to a resolution of 125 µm/voxel.

Around the coarse grains, sand S1, the presence of the interfacial transition zone (ITZ) is here taken into account. It is well-known that the ITZ is characterized by a higher concentration of portlandite and a much higher porosity than that of the bulk paste. Also, their mechanical properties are lower than those of the bulk paste. According to the literature, 20 µm seems to be a realistic value for ITZ thickness [30,31].

Table 5
Young's modulus values and variations of the different leached paste zones

E in Gpa					
	Zone 1	Zone 2	Zone 3	Zone 4	Zone 5
28 days	22.89	14.63	12.22	2.56	1.54
56 days	22.89	14.63	11.51	1.71	0.74
98 days	22.89	14.63	10.43	0.89	0.25
E/E_{sound}					
28 days	1	0.64	0.53	0.11	0.07
56 days	1	0.64	0.50	0.07	0.03
98 days	1	0.64	0.46	0.04	0.01

Table 6
Young's modulus values and variations of the different leached mortar zones — $E_{ITZ}/E_{bulk}=100\%$

E in Gpa ($E_{ITZ}/E_{bulk}=100\%$)					
	Zone 1	Zone 2	Zone 3	Zone 4	Zone 5
28 days	42.46	35.06	32.37	20.66	19.25
56 days	42.46	35.06	31.57	19.86	12.74
98 days	42.46	35.06	30.30	13.97	9.35
E/E_{sound}					
28 days	1	0.83	0.76	0.49	0.45
56 days	1	0.83	0.74	0.47	0.30
98 days	1	0.83	0.71	0.33	0.22

However, the regular mesh composed of cubic 125 µm side finite elements implies to affect homogenised properties. Compared to the lack of data on tensile strength and inelastic behaviour of ITZ, the literature is more abundant on the elastic properties of this phase. Then the elastic modulus of ITZ is assumed to be 50% of that of the bulk cement paste [31,32]. The results are compared to those where the ITZ is not taken into account in order to perform a sensitivity analysis on the elastic properties of this zone. Tables 6 and 7 give the calculated Young's moduli obtained for the 11 mortar zones for respectively $E_{ITZ}/E_{bulk}=100\%$ (ITZ is replaced by bulk paste) and $E_{ITZ}/E_{bulk}=50\%$.

The results clearly show that leaching affects directly the elastic modulus of both cement paste and mortar. However this effect is less high at the meso-scale (mortar) than at the micro-scale (cement paste) because of the presence of sands. The leaching of portlandite induces a decrease of 17% at the meso-scale against 36% at the micro-scale. This decrease is significantly higher when we take into account the dissolution of hydrated aluminates and sulfoaluminates phases and the C–S–H decalcification.

The effect of ITZ is also presented in Tables 6 and 7. No significant influence of ITZ on the Elastic Modulus value for the sound and leached mortar is observed.

3.2.3. Homogenised Young's modulus of the mortar sample

The modelling carried out in this study allows the prediction of elastic modulus of mortar sample at different degradation

Table 7
Young's modulus values and variations of the different leached mortar zones — $E_{ITZ}/E_{bulk}=50\%$

E in GPa ($E_{ITZ}/E_{bulk}=50\%$)					
	Zone 1	Zone 2	Zone 3	Zone 4	Zone 5
28 days	42.29	34.93	32.24	20.60	19.20
56 days	42.29	34.93	31.53	19.81	12.72
98 days	42.29	34.93	30.19	13.95	9.34
E/E_{sound}					
28 days	1	0.83	0.76	0.49	0.45
56 days	1	0.83	0.75	0.47	0.30
98 days	1	0.83	0.71	0.33	0.22

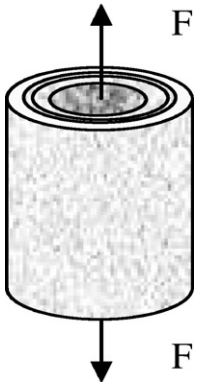

Fig. 13. Parallel model for mechanical test.

times (28, 56, 98 days). The following analytical relation Eq. (1) using a parallel model is considered (Fig. 13):

$$E_{\text{sample}} = \sum_i \frac{S_i}{S_{\text{tot}}} E_i. \quad (1)$$

Where E_i and S_i are the elastic modulus and the surface area of the zone i; S_{tot} is the total surface area.

Table 8 compares the predicted values of the Elastic modulus with the experimental ones for the unleached and leached mortars when ITZ is neglected. Table 9 gives the results when ITZ is taken into account. The results are plotted on a graph experimental vs. modelled results (Fig. 14).

The predicted and experimental values of the elastic modulus are in a good agreement. The proposed modelling allows the prediction of the elastic modulus of the different zones of the leached zone which is difficult to determine experimentally. The good agreement between experimental and numerical results shows the relevance of the chosen modelling.

4. Conclusion

A 3D multi-scale modelling of mechanical properties of cement-based materials approach is presented. The proposed approach provides a quantitative means to estimate and predict the mechanical properties of cement based materials taking into account the eventual changes in the micro-structure.

It consists in combining two modern numerical tools. First the NIST's 3D model (CEMHYD3D) is used to generate a realistic 3D Representative Volume Element of cement-based materials at 2 different scales (cement paste and mortar). The voxelized images are then converted to Finite Elements Meshes compatible with the FE software Abaqus. This last one is then used to study the mechanical behaviour of the considered 3D Representative Elementary Volume. The outcome of a lower scale is then used as input at a higher scale.

The proposed approach is firstly applied to determine the mechanical behaviour of a specific mortar with water-to-cement ratio 0.4 that is previously investigated experimentally. The micro-scale of the cement paste and the meso-scale of the mortar under tensile and compression loadings are investigated. Compared to the experimental results, elastic parameters and strength are correctly represented; non-linearities are well described, crack patterns before and after the peak are very realistic.

The approach is secondly applied to investigate the evolution of the elastic modulus of the specific mortar submitted to leaching by ammonium nitrate solution. The results show that leaching affects directly the elastic modulus of both cement paste and mortar. This effect is less high at the meso-scale (mortar) than at the micro-scale (cement paste) because of the presence of sands. The leaching of portlandite induces a decrease of 17% at the meso-scale against 36% at the micro-scale. This decrease is significantly higher when we take into account the dissolution of hydrated aluminates and sulfoaluminates phases and the C–S–H decalcification. However, no

Table 8
Comparison between modelling and experimental results (on Young's modulus) — $E_{\text{ITZ}}/E_{\text{bulk}}=100\%$

	E_{sample} in Gpa		$E_{\text{sample}}/E_{\text{sound}}$	
	Modelling	Experiment	Modelling	Experiment
0 days	42.46	44.55	1	1
28 days	34.19	34.32	0.80	0.77
56 days	29.31	28.65	0.69	0.64
98 days	23.56	21.1	0.55	0.47

Table 9
Comparison between modelling and experimental results (on Young's modulus) — $E_{\text{ITZ}}/E_{\text{bulk}}=50\%$

	E_{sample} in GPa		$E_{\text{sample}}/E_{\text{sound}}$	
	Modelling	Experiment	Modelling	Experiment
0 days	42.29	44.55	1	1
28 days	34.06	34.32	0.80	0.77
56 days	29.21	28.65	0.69	0.64
98 days	23.49	21.1	0.55	0.47

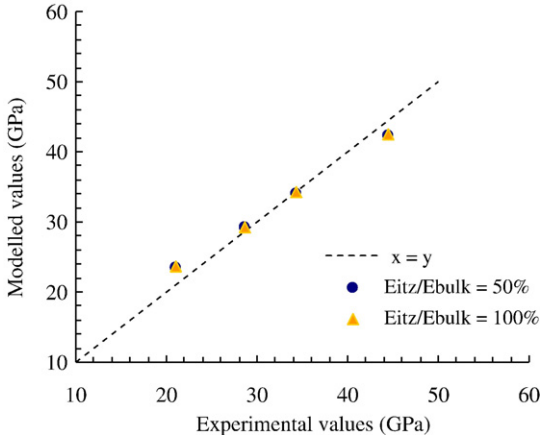

Fig. 14. Influence of leaching on Young modulus of mortar. Modelled results vs. experimental results.

significant influence of ITZ on the Elastic Modulus value for the sound and leached mortar is observed. The proposed modelling allows the prediction of the elastic modulus of the different zones of the leached zone which is difficult to determine experimentally.

The good agreement between experimental and numerical results shows the relevance of the proposed modelling. This approach will be extended to investigate the concrete scale as well as the influence of water-to-cement ratio, mineral additions.

Acknowledgement

The authors would like to acknowledge Dale Bentz, Edward Garboczi and Jeffrey Bullard for their help in using CEMHYD3D.

References

[1] G. Cailletaud, S. Forest, D. Jeulin, F. Feyel, I. Galliet, V. Mounoury, S. Quilici, Some elements of microstructural mechanics, Computational Materials Science 27 (3) (2003) 351–374.
[2] J. Wang, 1994, Development and application of a micromechanics-based numerical approach for the study of crack propagation in concrete, EPFL, Lausanne (Suisse), PhD Thesis.
[3] G. Mounajed, Exploitation du nouveau modèle « Béton numérique dans Symphonie, Concept, homogénéisation du comportement thermomécanique des BHP et simulation de l'endommagement thermique Cahiers du CSTB, 2002 (in French).
[4] I. Comby, P.-O. Bouchard, F. Bernard, F. Bay, E. Garcia-Diaz, 3D damage and discrete crack propagation modelling — application to the Alcali-Silica reaction at mesoscale in concrete structures, 9th European Mechanics of Materials Conference, Moret-sur-Loing, May 9–12, 2006.
[5] K. Van Breugel, Numerical simulations of hydratation and microstructural development in hardened cement paste — Part I: theory, Cement and concrete Research 25 (2) (1995) 319–331.
[6] E. Schlangen, E. Garboczi, Fracture simulations of concrete using lattice models: computational aspects, Engineering Fracture Mechanics 57 (2–3) (1997) 319–332.
[7] E. Schlangen, E.A.B. Koenders, K. Van Breugel, Influence of internal dilation on the fracture behaviour of multi-phase materials, Engineering Fracture Mechanics 74 (1–2) (2007) 18–33.
[8] M.M. Abreu, J.V. Lemos, J. Carmeliet, E. Schlangen, Modelling compressive cracking in concrete by a modified lattice model, in: Carpinteri, et al., (Eds.), Proceedings of the 6th International Conference on Fracture Mechanics of Concrete and Concrete Structures, New trends in Fracture Mechanics of Concrete, vol.1, Taylor & Francis Group, 2007, pp. 453–460.
[9] S. Kamali, Identification de la loi de comportement mécanique d'un mortier lixivié par du nitrate d'ammonium. Ecole Normale Supérieure de Cachan, France, Master report (in French), 1999.
[10] C. Le Bellégo, 2001, Couplage chimie mécanique dans les structures en béton armé attaquées par l'eau — Etude expérimentale et analyse numérique. LMT-ENS de Cachan, France, PhD Thesis (in French).
[11] D.P. Bentz, Three-dimensional computer simulation of portland cement hydration and microstructure development, Journal of American Ceramic Society 80 (1) (1997) 3–21.
[12] S. Kamali, 2003, Comportement et simulation des matériaux cimentaires en environnements agressifs: lixiviation et temperature, LMT-ENS de Cachan, France, PhD Thesis (in French).
[13] T. Kanit, S. Forest, I. Galliet, V. Mounoury, D. Jeulin, Determination of the size of the representative volume element for random composites: statistical and numerical approach, International Journal of Solids and Structures 40 (13–14) (2003) 3647–3679.
[14] V. Smilauer, 2005. Elastic properties of hydrating cement paste determined from hydratation methods. University of Prague, Czech Republic, PhD thesis.
[15] Abaqus v.6.6., Documentation, User's Manual — Part V: Materials, 2006.
[16] S. Kamali, M. Moranville, E. Garboczi, S. Prené, B. Gérard, Hydrate dissolution influence on the Young's modulus of cement pastes, Proceedings of the 5th International Conference on Fracture Mechanics of Concrete and Concrete Structures, 2004, pp. 631–638.
[17] A. Boumiz, D. Sorrentino, C. Vernet, F. Tenoudji, Modelling the development of the elastic moduli as a function of the degree of hydration of cement pastes and mortars, in: A. Nonat (Ed.), Proceedings 13 of the 2nd RILEM Workshop on Hydration and Setting: Why Does Cement Set ? An Interdisciplinary Approach, RILEM, Dijon, 1997.
[18] M.M. Choy, W.R. Cook, R.F.S. Hearmon, J. Jaff, J. Jerphagnon, S.K. Kurtz, S.T. Liu, D.F. Nelson, in: K.-H. Kellwege, A.M. Hellwege (Eds.), Landolt-Bornstein: Numerical Data and Functional Relationships in Science and Technology New Series. Group III: Crystal and Solid State Physics, (Revised and extented edition of volume III/1 and III/2), Elastic, Piezoelectric, Pyroelectric, Piezooptic, Electrooptic constants, and nonlinear dielectric susceptibilities of crystals, vol. 11, Springer-Verlag, Berlin, 1979.
[19] A.S. Bhalla, W.R. Cook, R.F.S. Hearmon, J. Jerphagnon, S.K. Kurtz, S.T. Liu, D.F. Nelson, J.L. Oudar, in: K.-H. Kellwege, A.M. Hellwege (Eds.), Landolt-Bornstein: Numerical Data and Functional Relationships in Science and Technology New Series, Group III: Crystal and Solid State Physics, (Supplement to volume III/11), Elastic, Piezoelectric, Pyroelectric, Piezooptic, Electrooptic Constants, and nonlinear dielectric susceptibilities of crystals, vol. 18, Springer-Verlag, Berlin, 1984.
[20] P.J.M. Monteiro, C.T. Chang, The elastic moduli of calcium hydroxide, Cement and Concrete Research 25 (1995) 1605–1609.
[21] D. Damidot, K. Velez, F. Sorrentino, Characterisation of interstitial transition zone (ITZ) of high performance cement by nanoindentation technique, 11th International Congress on the Chemistry of Cement, Durban, 2003.
[22] A. Hillerborg, M. Modeer, P.E. Petersson, Analysis of crack formation and crack growth in concrete by means of fracture mechanics and finite elements, Cement and Concrete Research 6 (6) (1976) 773–782.
[23] A. Menou, 2004, Etude du comportement thermomécanique des bétons à haute température: approche multiéchelles de l'endommagement thermique, Université de Pau et des Pays de l'Adour, France, PhD Thesis (in French).
[24] Z. Agioutantis, E. Chatzopoulou, M. Stavroulaki, A numerical investigation of the effect of the interfacial zone in concrete structures under uniaxial compression, Cement and Concrete Research 30 (5) (2000) 715–723.
[25] T. Akçaoglu, M. Tokyay, T. Çelik, Assessing the ITZ microcracking via scanning electron microscope and its effect on the failure behavior of concrete, Cement and Concrete Research 35 (2) (2005) 358–363.
[26] C. Carde, 1996, Caractérisation et modélisation de l'altération des propriétés mé- caniques due à la lixiviation des matériaux cimentaires, INSA de Toulouse, France, PhD Thesis (in French).
[27] P.H. Heukamp, F.J. Ulm, J.T. Germaine, Mechanical properties of calcium leached cement pastes: triaxial stress and the influence of the pore pressure, Cement and Concrete Research 31 (5) (2001) 767–774.
[28] F. Adenot, 1992, Durabilité du béton: Caractérisation et modélisation des proces- sus physiques et chimiques de dégradation du ciment, Université d'Orléans, France, PhD Thesis (in French).
[29] V. Matte, M. Moranville, Durability of reactive powder composites: influence of silica fume on the leaching properties of very low water/binder pastes, Cement and Concrete Composites 21 (1999) 1–9.
[30] B. Bourdette, 1994, Durabilité du mortier: prise en compte des auréoles de transi- tion dans la caractérisation et la modélisation des processus physiques et chimi- ques d'altération. INSA de Toulouse, France. PhD Thesis (in French).
[31] C.C. Yang, Effect of the transition zone on the elastic moduli of mortar, Cement and Concrete Research 28 (5) (1998) 727–736.
[32] E. d. Garboczi, D.P. Bentz, Analytical formulas for interfacial transition zone properties, Advanced Cement Based Materials 6 (3–4) (1997) 99–108.